



**HAL**  
open science

## Semiempirical in-cylinder pressure based model for NOX prediction oriented to control applications

C. Guardiola, J.J. López, J. Martin, D. García-Sarmiento

► **To cite this version:**

C. Guardiola, J.J. López, J. Martin, D. García-Sarmiento. Semiempirical in-cylinder pressure based model for NOX prediction oriented to control applications. Applied Thermal Engineering, 2011, 10.1016/j.applthermaleng.2011.05.048 . hal-00789885

**HAL Id: hal-00789885**

**<https://hal.science/hal-00789885v1>**

Submitted on 19 Feb 2013

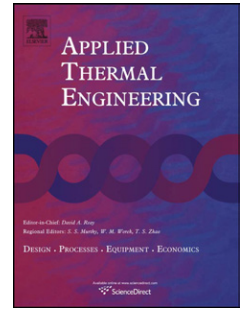
**HAL** is a multi-disciplinary open access archive for the deposit and dissemination of scientific research documents, whether they are published or not. The documents may come from teaching and research institutions in France or abroad, or from public or private research centers.

L'archive ouverte pluridisciplinaire **HAL**, est destinée au dépôt et à la diffusion de documents scientifiques de niveau recherche, publiés ou non, émanant des établissements d'enseignement et de recherche français ou étrangers, des laboratoires publics ou privés.

# Accepted Manuscript

Title: Semiempirical in-cylinder pressure based model for NOX prediction oriented to control applications

Authors: C. Guardiola, Ph.D J.J. López, Ph.D J. Martin, Ph.D D. García-Sarmiento



PII: S1359-4311(11)00316-4

DOI: [10.1016/j.applthermaleng.2011.05.048](https://doi.org/10.1016/j.applthermaleng.2011.05.048)

Reference: ATE 3601

To appear in: *Applied Thermal Engineering*

Received Date: 22 September 2010

Revised Date: 20 May 2011

Accepted Date: 31 May 2011

Please cite this article as: C. Guardiola, J.J. López, J. Martin, D. García-Sarmiento. Semiempirical in-cylinder pressure based model for NOX prediction oriented to control applications, *Applied Thermal Engineering* (2011), doi: 10.1016/j.applthermaleng.2011.05.048

This is a PDF file of an unedited manuscript that has been accepted for publication. As a service to our customers we are providing this early version of the manuscript. The manuscript will undergo copyediting, typesetting, and review of the resulting proof before it is published in its final form. Please note that during the production process errors may be discovered which could affect the content, and all legal disclaimers that apply to the journal pertain.

## Semiempirical in-cylinder pressure based model for NO<sub>x</sub> prediction oriented to control applications

### Highlights

- A NO<sub>x</sub> predictive model oriented to control applications has been proposed.
- In-cylinder pressure has been used as a basic input signal for NO<sub>x</sub> prediction.
- The model proposed combines a fast physical-based model with empirical look-up tables.
- The model considers NO<sub>x</sub> formation and NO<sub>x</sub> reduction phenomena.
- The model total calculation time is smaller than an engine cycle.

## Semiempirical in-cylinder pressure based model for $\text{NO}_x$ prediction oriented to control applications

C. Guardiola, J.J. López, J. Martín\*, D. García-Sarmiento

*CMT-Motores Térmicos, Universitat Politècnica de València, Camino de Vera s/n, 46022, Valencia, Spain*

---

### Abstract

This work describes the development of a fast  $\text{NO}_x$  predictive model oriented to engine control in diesel engines. The in-cylinder pressure is the only instantaneous input signal required, along with several mean variables that are available in the ECU during normal engine operation.

The proposed model is based on the instantaneous evolution of the heat release rate and the adiabatic flame temperature (both obtained among other parameters from the in-cylinder pressure evolution). Corrections for considering the  $\text{NO}_x$  reduction due to the re-burning mechanism are also included. Finally, the model is used for providing a model-based correction of tabulated values for the  $\text{NO}_x$  emission at the reference conditions. The model exhibits a good behaviour when varying exhaust gas recirculation rate, boost pressure and intake temperature, while changes in the engine speed and injection settings are considered in the tabulated values.

Concerning the calculation time, the model is optimized by proposing simplified sub-models to calculate the heat release and the adiabatic flame temperature. The final result is suitable for real time applications since it takes less than a cycle to complete the  $\text{NO}_x$  prediction.

*Keywords:*  $\text{NO}_x$ , heat release rate, adiabatic flame temperature, re-burning

---

---

\*Corresponding author. Tel: +34963877650; fax: +34963877659

Email address: [jaimardi@mot.upv.es](mailto:jaimardi@mot.upv.es) (J. Martín)

URL: [www.cmt.upv.es](http://www.cmt.upv.es) (J. Martín)

## Nomenclature

$c_v$	specific heat at constant volume	[J/kg K]
$dQ_b$	heat release rate	[W]
ECU	engine control unit	
EGR	exhaust gas recirculation	[%]
EOC	end of combustion	[°]
FFT	fast Fourier transform	
$F_r$	fuel-air equivalence ratio	[-]
$h$	specific enthalpy	[J/kg]
<b>IVC</b>	intake valve closing	
K	constant	
$m$	mass	[kg]
$n$	engine speed	[rpm]
<b><math>NO_x</math></b>	nitrogen oxides	[mg/str]
$p$	pressure	[bar]
$Q$	heat transfer to the walls and heat release	[J]
$R$	specific gas constant	[J/kg K]
SOC	start of combustion	[°]
SOI	start of injection	[°]
T	temperature	[K]
$u$	specific internal energy	[J/kg]
V	volume	[m <sup>3</sup> ]
$y$	mass fraction	[-]

## Subscripts

$0$	reference operating conditions
$a$	air
$ad$	adiabatic
$b$	stoichiometric combustion products
$base$	base model
$bb$	<i>blow-by</i>
$c$	gas mean properties in the chamber
$comb$	current combustion
$cyl$	in-cylinder
$diss$	dissociation
$exh$	exhaust manifold
$exp$	experimental measurements
$f$	fuel
$f, ev$	fuel evaporation
$f, g$	gaseous fuel
$f, inj$	liquid fuel at injection conditions
$inj$	injection
$itk$	intake manifold
$main$	main injection
$net$	net production at current cycle
$nd$	non-dissociated species
$O_2$	oxygen
$pil$	pilot injection
$re$	re-burning
$ub$	unburned gas

## Greek symbols

$\alpha$	crank angle
$\gamma$	adiabatic coefficient
$\epsilon$	NO <sub>x</sub> reduction efficiency

## 1. Introduction

The compression ignition engine is today the most efficient engine for transport applications in terms of fuel consumption; nevertheless its pollutant emissions still represent a major environmental challenge. For the implementation of active control methods, and also the control of after-treatment systems, a proper modelling of the pollutants production can be a reliable alternative to the gas composition sensors that are being developed [1, 2]. One of the main pollutants in compression ignition engines are nitrogen oxides (NO<sub>x</sub>). NO<sub>x</sub> are produced during basically all kinds of combustions and their formation can be divided into four different types: thermal NO<sub>x</sub> formation, fuel NO<sub>x</sub>

10 formation, prompt  $\text{NO}_X$  formation and finally via  $\text{N}_2\text{O}$ . As it will be justified, this work  
11 is focused only on the thermal  $\text{NO}_X$  production.

12 Several models that predict the amount of  $\text{NO}_X$  emission released by diesel engines  
13 have been published [3–6]. Some of them are based on correlations of the  $\text{NO}_X$  production  
14 with different operation variables [7], while others account for the in-cycle evolution of  
15 the  $\text{NO}_X$ . Between these last, some of them use the in-cylinder pressure signal as an  
16 input quantity [3, 8, 9]. The in-cylinder pressure is considered a valuable signal because  
17 it provides direct information of the combustion development, as for example the peak  
18 pressure or the indicated mean effective pressure. Moreover, in-cylinder pressure can  
19 allow some more complex engine control applications such as air mass flow estimation  
20 [10], on-line combustion detection [11] or failure detection [12], exhaust gas recirculation  
21 control [13], torque estimation [14] or noise control [15]. In this work, in-cylinder pressure  
22 will be used as a basic input signal for predicting the  $\text{NO}_X$  emission for control oriented  
23 applications, on the basis of the calculation of the heat release and the adiabatic flame  
24 temperature during the combustion process.

25 Although this kind of models that track the instantaneous  $\text{NO}_X$  production suppose a  
26 non negligible computational burden, recent evolution in the control unit computational  
27 power makes it possible apply them for the engine control and diagnosis. In that sense  
28 [8, 9, 16] have proposed models that integrate reliable  $\text{NO}_X$  estimations with almost real  
29 time calculations. The use of these fast predictive models combined with closed-loop  
30 control of the injection settings and air loop control settings has a big potential on novel  
31 technologies oriented for both diminishing  $\text{NO}_X$  production during combustion as well as  
32 improving  $\text{deNO}_X$  aftertreatment. As an example, there are some works [17, 18] in which  
33  $\text{NO}_X$  prediction models allows to optimise the control of the reduction agent flow into  
34 the catalytic converter, using only the minimum necessary amount and thus extending  
35 its lifetime.

36 A key issue when dealing with  $\text{NO}_X$  prediction models oriented to control applications  
37 is to maintain a good equilibrium between accuracy and calculation time. Regarding this  
38 point two extreme options can be considered: physical modelling approach, or experi-  
39 mental mapping of the  $\text{NO}_X$  emitted by a reference engine as a function of engine speed  
40 and load. The first option provides a physical representation of the problem, providing  
41 prediction capabilities when the engine is in off-design operation, while the second option  
42 has clear computational advantages, and also can be more precise as far as the engine  
43 operation is close to the nominal situation.

44 The model proposed in this work combines a fast physical-based model and a set of  
45 empirical look-up tables with the reference values for the nominal conditions. Tabulated  
46 values are used for providing a nominal value of the  $\text{NO}_X$  production, while heat release  
47 profile and the adiabatic flame temperature are calculated from in-cylinder pressure and  
48 their evolution is then compared with the nominal situation to provide a  $\text{NO}_X$  correc-  
49 tion to be applied. Additionally, the proposed model does not only consider the  $\text{NO}_X$   
50 formation, but its reduction when  $\text{NO}_X$  molecules are re-entrained in the spray (known  
51 in the literature as re-burning [1]).

52 The paper is structured as follows: section 2 provides a description of the engine and  
53 the experimental set-up used to obtain the data for the model development. Section 3,  
54 4 and 5 are devoted to the description of the base  $\text{NO}_X$  model, the correction due to the  
55 re-burning process and the approach used for the online calculation respectively. Finally  
56 sections 6, 7 and 8 present the model validation and discussion, some computational

57 issues and the main conclusions.

## 58 2. Experimental Setup

59 A schema of the test cell layout with the instrumentation is shown in Figure 1. The  
60 experimental tests were carried out in a high speed direct injection diesel engine with  
61 2.2-litre of total displacement that is currently in production. It is a four-cylinder engine  
62 with sequential parallel turbo-charger [19] equipped with a Bosch common rail injection  
63 system. The engine main characteristics are given in Table 1.

64 The in-cylinder pressure was measured in one of the cylinders by means of a Kistler  
65 6055B glow-plug piezoelectric transducer, with a range between 0 and 250 bar and a  
66 sensitivity of 18.8 pC/bar. The pressure sensor was calibrated according to the traditional  
67 method proposed in [20]. Angle-synchronous acquisition was used for the in-cylinder  
68 pressure. For this purpose an optical encoder providing two signals was used: the first  
69 is a pulse at each crankshaft revolution, which is used as trigger signal; the second is an  
70 external clock for the instantaneous acquisition system with a  $0.5^\circ$  sampling interval. The  
71 trigger, the external clock and the in-cylinder pressure signals are fed to the acquisition  
72 system, a Yokogawa DL708E oscillographic recorder. Several mean variables (acquired at  
73 a constant sample frequency of 100 Hz) are necessary for controlling the engine operating  
74 point and also for the model calculation; an AVL tests system is used for this purpose.  
75 The values of the inlet pressure and temperature **along with the fresh air mass flow** were  
76 also collected from the ECU. The exhaust emissions were analysed and recorded using  
77 an exhaust monitoring equipment (Horiba MEXA 7100 D), and the intake manifold  $\text{CO}_2$   
78 concentration was also measured for determining the EGR rate.

79 The comparison between the mean values obtained from the AVL tests system and the  
80 engine ECU showed a mean relative error of about 2%. Such difference was considered  
81 small enough to use directly the ECU values, which is coherent with the aim of the model,  
82 that is, to be used in control applications.

83 For the definition of the test matrix the variables affecting  $\text{NO}_X$  and the foreseen  
84 application of the model were considered. According to [21, 22], the parameters affecting  
85  $\text{NO}_X$  formation can be grouped into two possible sources: the intake conditions ( $T_{itk}$ ,  
86  $p_{itk}$  and gas composition depending on the EGR rate) and fuel injection parameters  
87 (injection pressure  $-p_{inj}$ -, injection strategies: start of main injection  $-\text{SOI}_{main}$ - and  
88 pilot injection  $-\text{SOI}_{pil}$ -). Molina [22] performed a sensitivity study of  $p_{inj}$  and  $\text{SOI}_{main}$ ,  
89 evaluating their influence over  $\text{NO}_X$  emissions. He concluded that  $p_{inj}$  is more effective  
90 than  $\text{SOI}_{main}$ , since for the same  $\text{NO}_X$  reduction (respect to the nominal value) the  
91 penalty in fuel consumption is smaller than modifying the injection timing ( $\text{SOI}_{main}$  must  
92 allow a centred combustion in order to maximise the engine performance, and  $\text{SOI}_{pil}$  is  
93 optimized according to combustion noise restrictions). If a parametric variation of the  
94 injection parameter is considered, this conclusion would allow to rank those parameters  
95 according of their influence.

96 Nevertheless, the model is intended to be used for the control of current diesel engines,  
97 where injection settings are programmed as a function of engine load and speed. Hence  
98 the experimental plan will be based on the assumption that the injection settings are  
99 fixed, while parametric studies are run for EGR rate, intake pressure  $p_{itk}$  and intake  
100 temperature  $T_{itk}$ . Such variations are similar to those occurring during load and speed  
101 transients during realistic engine operation.



102 Figure 2 summarises the variation ranges for the experimental tests; the data set  
 103 has been divided into a training data set and a validation data set. The experimental  
 104 plan included 14 reference operating points at different speeds and loads for the model  
 105 development and 23 for its validation, as shown in Table 2. At each operating point,  
 106 variations of the EGR rate (from 0% to 58% EGR at low load and up to 25% at high  
 107 load), the boost pressure (up to 1 bar variation with regard to the nominal operation)  
 108 and inlet temperature (up to 40 K variation) were performed. **It is important to highlight  
 109 that each parametric variation was performed at constant fuel mass; hence, for the sake  
 110 of clarity, only the nominal points have been included at the left of Figure 2.**

### 111 3. Base $\text{NO}_X$ model

112 In this section the basic  $\text{NO}_X$  model is presented. This model will be reformulated  
 113 in section 5 in order to be used as a corrective factor based on the measured in-cylinder  
 114 pressure. The basic model is based on the one presented by Arrègle *et al.* [9] which, in  
 115 order to increase its reliability and accuracy, has been modified with an improved heat  
 116 release calculation (which will be presented in section 3.1) and the inclusion of a  $\text{NO}_X$   
 117 emission correction based on re-burning mechanism (shown in section 4).

118 Although the basic model is based on the  $\text{NO}$  formation, rather than the  $\text{NO}_X$ , in  
 119 this work we will refer generically to  $\text{NO}_X$  because  $\text{NO}$  formation and  $\text{NO}_X$  emission are  
 120 assumed to be correlated, and because the final model will be adjusted to fit experimen-  
 121 tal tailpipe  $\text{NO}_X$  emissions. Hence, no specific distinction will be made between both  
 122 quantities.

123 The basic model in [9] is based on the Zeldovich thermal  $\text{NO}_X$  mechanism [23, 24].  
 124 The  $\text{NO}_X$  formation is exponentially dependent on temperature, **and thus local high  
 125 temperature in the flame, caused by the non-homogeneous nature of diesel combustion  
 126 [25], can have a very large impact on the quantity of  $\text{NO}_X$  produced.** However, a complete  
 127 tracking of the  $\text{NO}_X$  kinetic is discarded because two reasons:

- 128 • It seems incompatible with the ECU computation capability; this could be solved  
 129 using a parametrisation of the Zeldovich mechanism, reducing the computation  
 130 requirements [26].
- 131 • A complete tracking makes no sense without a proper description of the flame.  
 132 This second issue is out of the scope of a control oriented model.

133 On the one hand, the original basic model [9] assumes that the main  $\text{NO}_X$  production  
 134 takes place at the highest temperatures in the chamber [27], and thus the most suitable  
 135 variable to account for the  $\text{NO}_X$  formation is the adiabatic flame temperature ( $T_{ad}$ ).  
 136 This correlation between adiabatic temperature and nitric oxide production can also be  
 137 found at other works [28].

138 On the other hand, the original approach considers that fuel burns at stoichiometric  
 139 fuel/air equivalence ratio ( $F_r = 1$ ), where the temperature is close to the adiabatic  
 140 temperature. Thus, it is directly derived that the formation of combustion products, and  
 141 thus  $\text{NO}_X$ , is correlated with the instantaneous heat release rate ( $dQ_b$ ).

142 From these two hypotheses, the base  $\text{NO}_X$  model according to [9] is:

$$m_{NO_x,base} = \int_{\alpha} dQ_b(\alpha) \cdot K_1 \cdot \left(\frac{n}{2000}\right)^{K_2} \cdot e^{\left(\frac{K_3}{T_{ad}(\alpha)}\right)} d\alpha \quad (1)$$

143 where  $m_{NO_x,base}$  is the total predicted  $NO_x$  mass per cycle,  $n$  is the engine speed and  $K_1$ ,  
 144  $K_2$  and  $K_3$  are constants that have to be experimentally fitted. A complete description  
 145 of the  $K_1$ ,  $K_2$  and  $K_3$  fitting process will be provided in section 3.3; however, for the  
 146 sake of comprehension it is interesting to highlight at this point that  $K_1$  has a positive  
 147 value while both  $K_2$  and  $K_3$  are negative.

148 According to [29] the term including the engine speed is due to the fact that at higher  
 149 engine speeds fuel is consumed in a much shorter time period by the enhanced fuel/air  
 150 mixing process, shortening the combustion duration providing less available time for  
 151  $NO_x$  formation.

### 152 3.1. Heat release rate calculation

153 The heat release rate is the rate at which the chemical energy of the fuel is released  
 154 by the combustion process and, as stated in equation (1)  $dQ_b$  is proportional to  $NO_x$   
 155 formation.  $dQ_b$  can be calculated from in-cylinder pressure, with different levels of  
 156 complexity and accuracy [30, 31]. In the previous work [9] the heat release was calculated  
 157 with a fast heat release expression based on the first law of thermodynamics. This kind  
 158 of calculation is very suitable for the ECU capabilities but it has an important effect on  
 159 the accuracy of the predictions, as it will be shown later. Thus, for the sake of precision,  
 160 a more complex, and hence slightly slower, calculation is proposed. It is an evolution of  
 161 the combustion diagnosis model CALMEC [32–34], an in-house code for calculating the  
 162 heat release.

163 The main input of the combustion diagnosis model is the in-cylinder pressure and  
 164 some mean variables available in the ECU: air and fuel mass flows, temperature and  
 165 pressure in the manifolds, coolant temperature, engine speed and injection settings (start  
 166 and duration of each pulse).

167 The diagnosis model solves the first law and the gas equation of state between intake  
 168 valve closing (IVC) and exhaust valve opening to obtain the rate of heat released and the  
 169 instantaneous mean temperature in the chamber. For such calculation, the model consid-  
 170 ers that the pressure is uniform in the combustion chamber and the gas is assumed to be  
 171 a perfect mixture of three perfect gases (air, gaseous fuel and stoichiometric burnt prod-  
 172 ucts). Gas properties are calculated through correlations considering the mean chamber  
 173 temperature. The model also accounts for convective heat transfer to the walls [35, 36],  
 174 and blow-by leakage.

175 The final expression of the first law obtained is:

$$dQ_b = m_c c_{v,c} dT + dQ + p dV - (h_{f,inj} - u_{f,g}) \cdot dm_{f,ev} + R_c T_c dm_{bb} \quad (2)$$

176 where  $m_c$  is the mass of the mixture contained in the combustion chamber,  $c_{v,c}$  is the  
 177 specific heat at constant volume of the mixture,  $Q$  is the heat transferred to the walls,  $p$   
 178 and  $V$  are the in-cylinder pressure and volume,  $h_{f,inj}$  stands for the injected fuel specific  
 179 enthalpy and  $u_{f,g}$  for the gaseous fuel energy of the evaporated fuel mass  $m_{f,ev}$ . The  
 180 last term in the expression accounts for the blow-by leakage  $m_{bb}$ , characterised by the  
 181 combustion chamber specific gas constant  $R_c$  and mean temperature  $T_c$ .

182 In order to solve equation (2) several sub-models are combined [37]. Figure 3 illus-  
183 trates the calculation sequence of the different sub-models.

184 The initial simplified model for  $dQ_b$  calculation as used in [9] took about 2 ms per  
185 engine cycle in a 3 GHz PC, while the detailed calculation using the code presented  
186 in [32] consumed 484 ms, which was far away of a real-time application scenario. In  
187 order to overcome this problem, some of the sub-models with high computational cost  
188 were simplified or optimised. The main actions consisted on the elimination of some  
189 non-critical calculation sub-models (such as fuel evaporation), the substitution of slow  
190 sub-models (such as the filling-emptying model used to estimate the trapped mass) by  
191 others simpler and faster [38] and the simplification of the pressure processing (pressure  
192 pegging using the intake pressure instead of a thermodynamic criterion and fast filtering  
193 instead of FFT). With such strategies, the final time for calculating the  $dQ_b$  was about  
194 2.5 ms, near to the time consumed by the initial simplified model but providing a higher  
195 accuracy. The benefits of this improved accuracy will be demonstrated in section 5.

### 196 3.2. Calculation of the adiabatic flame temperature

197 The temperature in a combustion process in the absence of heat losses to the sur-  
198 roundings is commonly referred to as the adiabatic flame temperature, which corresponds  
199 to the maximum temperature that can be achieved for some given reactants, because any  
200 heat transfer or work from the reacting substances and any incomplete combustion would  
201 tend to lower the temperature of the products.

202 Figure 4 shows an schema of the procedure for calculating  $T_{ad}$  taking into account  
203 dissociation effects. From the known value of the air mass fraction at IVC,  $y_{a,IVC}$ , the  
204 oxygen mass fraction  $y_{O_2,IVC}$  can be directly derived. In addition to the gas composition,  
205 the other key variable for the adiabatic flame temperature calculation is the unburned  
206 gas temperature ( $T_{ub}$ ), which can be calculated assuming that the heat losses to the  
207 walls of the combustion chamber from the unburned gas and the heat transfer from the  
208 flame are equal. The unburned gas temperature at the start of combustion (SOC) is  
209 obtained from the thermodynamic diagnosis model. From this value, the instantaneous  
210  $T_{ub}$  is calculated with the expression of an isentropic compression:

$$T_{ub} = T_{ub-1} \cdot \left( \frac{p_{cyl}}{p_{cyl-1}} \right)^{\left( \frac{\gamma-1}{\gamma} \right)} \quad (3)$$

211 where  $p_{cyl}$ ,  $T_{ub}$ ,  $p_{cyl-1}$  and  $T_{ub-1}$  are the in-cylinder pressure and temperatures at the  
212 current angle and at the previous angle respectively.

213 Once  $y_{O_2,IVC}$  and  $T_{ub}$  evolution along the cycle are calculated, the following ex-  
214 pression is used for determining the adiabatic flame temperature during the diffusion  
215 combustion process [9]:

$$T_{ad}(\alpha) = T_{ub} + \Delta T_{nd}(\alpha) - \Delta T_{diss}(\alpha); \quad \Delta T_{nd} = 37630.5 \cdot \left( \frac{y_{O_2}}{3.48 \cdot F_r} \right) \quad (4)$$

$$\text{If } T_{ub} + \Delta T_{nd}(\alpha) < 2600K; \quad \Delta T_{diss}(\alpha) = 1.554 \cdot 10^{-7} \cdot (T_{ub} + \Delta T_{nd})^{2.677}(\alpha) \quad (5)$$

$$\text{If } T_{ub} + \Delta T_{nd}(\alpha) > 2600K; \quad \Delta T_{diss}(\alpha) = 7.136 \cdot 10^{-10} \cdot (T_{ub} + \Delta T_{nd})^{3.36}(\alpha) \quad (6)$$

216 where the combustion temperature is the result of the unburnt gas temperature  $T_{ub}$ , the  
 217 shift in the temperature due to the heat released during the combustion  $\Delta T_{nd}$ , and a  
 218 correction  $\Delta T_{diss}$  according to the expressions (5) and (6), that accounts for the energy  
 219 absorbed by the partial dissociation of the combustion products  $\text{CO}_2$ ,  $\text{H}_2\text{O}$ ,  $\text{N}_2$  and  $\text{O}_2$   
 220 into  $\text{CO}$ ,  $\text{H}_2$ ,  $\text{H}$ ,  $\text{OH}$ ,  $\text{O}$ ,  $\text{NO}$  and  $\text{N}$  (see [9] for further details).

221 As an illustrative example, Figure 5 shows the calculated evolution of the different  
 222 temperatures (unburnt gas temperature, flame temperature without considering species  
 223 dissociation and the adiabatic flame temperature) for one of the experimental test at  
 224 2500 rpm and 58% load. It must be highlighted that all the involved mechanisms are  
 225 significant and may not be neglected.

### 226 3.3. Fitting of the base $\text{NO}_x$ model constants

227 The fitting process consists on determining the values for  $K_1$ ,  $K_2$  and  $K_3$  in expression  
 228 (1). First step in this process is deciding if the general constant values will be fitted for  
 229 the whole operating range of the engine, or if a local optimisation will be used and then  
 230 the different constants are programmed as a function of a set of operating parameters  
 231 (as engine speed or load). Local fitting of the model can be also used for determining  
 232 the suitability of using the global approach. For that, an individual set of constants  
 233  $\{K_1, K_2, K_3\}$  is obtained for each nominal condition (considering the nominal test and  
 234 the parametric study performed for that engine speed and load).

235 Note that as engine speed is kept constant when varying EGR rate, boost pressure  
 236 and intake manifold temperature, it is not possible to provide an estimate for  $K_1$  and  
 237  $K_2$  independently but  $K_1 (n/2000)^{K_2}$  must be fitted as a group.

238 Figure 6 shows the values of the constants obtained in each operating condition tested  
 239 according to Table 2, for both training and validation operating points. Each point in  
 240 Figure 6 corresponds to the optimal selection of the model constants for minimising the  
 241 error of the group of tests obtained varying  $p_{itk}$ ,  $T_{itk}$  and EGR rate at a given engine  
 242 speed and load. As it can be appreciated  $K_3$  exhibits a quite constant value, while  
 243  $K_1 (n/2000)^{K_2}$  strongly depends on the operating conditions.

244 The model mean error is shown in Table 3 both in absolute and relative terms, using  
 245 training and validation experimental tests. The mean absolute error (columns 1 and 2)  
 246 is directly the mean value of the difference (not taking into account the sign) between  
 247 the model and the experimental data in  $\text{NO}_x$  units ( $\text{mg}/\text{str}$ ). The mean relative error  
 248 (columns 3 and 4) is the mean value of the relative error at each point (absolute error  
 249 divided by the experimental value) and it is a dimensionless number that allows to  
 250 standardise the range of deviation.

251 On the other hand, global constants can be fitted using a global approach. For  
 252 that, a least squares algorithm was used to obtain global values for  $\{K_1, K_2, K_3\}$ , using  
 253 only the data set corresponding to the training tests in Table 2. Then, these constants  
 254 were used for the whole operating range of the engine, for both training and validation  
 255 operating points. Figure 6 depicts the evolution of the fitted  $K_1 (n/2000)^{K_2}$  and  $K_3$ , and  
 256 its comparison with the local values. Mean estimate errors for the training and validation  
 257 data set are shown in the second row of Table 3.

258 Note that, according to Table 3, the local fit always provides more precise results than  
 259 the global fit of the model, which is straightforwardly derived from the fitting concept.  
 260 However, as the variation of  $K_3$  along the operation range of the engine is limited (the

261 variation coefficient is 0.7%), it is possible to consider a global  $K_3$  while using a local fit of  
 262 the two other model coefficients. Such approach will be considered in section 5. It is also  
 263 interesting to highlight that the mean absolute errors obtained with the validation data  
 264 are **much** higher than those obtained using the training data **while the mean relative**  
 265 **errors are similar**. This is because the model was trained with operating conditions  
 266 ranging from idle to 3000 rpm at partial loads, where the  $\text{NO}_X$  produced are low (less  
 267 than 2 mg/str) in comparison to the whole engine map (up to 8.5 mg/str at full load and  
 268 high speed) that was used for the validation. This issue will be discussed in section 6.

269 Figure 7 shows an example of the predicted vs. experimental  $\text{NO}_X$  emissions obtained  
 270 in a parametric variation of EGR rate, boost pressure and intake temperature, after the  
 271 described local fit approach. Two operating points at 2000 rpm are represented, one at  
 272 very low load (15%) and the other at medium-high load (58%). As can be seen the model  
 273 is able to correctly predict the trends in the  $\text{NO}_X$  when a variation in any of the three  
 274 parameters is performed. The observed trends can be easily justified:

- 275 • EGR variation: according to Ladommatos *et al.* [21], when the exhaust gases  
 276 are recirculated the displacement of inlet charge with  $\text{CO}_2$  and  $\text{H}_2\text{O}$  affects the  
 277 combustion process through three main effects: thermal, dilution and chemical  
 278 effect. The greater reduction of  $\text{NO}_X$  emissions is reached by the thermal effect,  
 279 and it is mainly because when the  $y_{\text{O}_2}$  goes down in the combustion chamber, the  
 280  $T_{ad}$  decreases too, directly influencing the  $\text{NO}_X$  production. **This trend is enhanced**  
 281 **when the EGR rate increases [39].**
- 282 •  $T_{itk}$  variation: the intake temperature was progressively raised from 336 to 360K,  
 283 keeping  $p_{itk}$  constant. This parameter increases the  $\text{NO}_X$  level due to two effects.  
 284 First a variation of  $T_{itk}$  directly affects  $T_{ad}$  through  $T_{ub}$  (as explained in section 3.2),  
 285 the second is a reduction of the ignition delay and, thus the combustion is advanced,  
 286 raising the gas temperature  $T_{ub}$ .
- 287 •  $p_{itk}$  variation: in agreement with the equation of state, when the pressure is in-  
 288 creased (maintaining  $T_{itk}$  constant), the density also increases thus improving the  
 289 air-fuel mixture thus accelerating the combustion and also increasing the gas tem-  
 290 perature  $T_{ub}$ . Additionally when the boost pressure increases (keeping the inlet  
 291 temperature and the EGR rate) the fresh air mass flow increases and therefore air-  
 292 fuel ratio gets lower, thus increasing the oxygen composition and  $T_{ad}$ . As a result  
 293 of these variations,  $\text{NO}_X$  emissions increases significantly.

294 According to Figure 7 it can be stated that the model behaves better when EGR vari-  
 295 ations are introduced, since it has the lowest error. This trend is also followed at different  
 296 operating points, with a mean relative error of 13.2% in the EGR variations versus 18.4%  
 297 in the  $p_{itk}$  and 21.3% in the  $T_{itk}$  parametric studies. This can be attributed to the model  
 298 sensitivity to changes in  $T_{ad}$  which is directly related to  $y_{\text{O}_2,IVC}$ . The influence of the  
 299 EGR rate over  $T_{ad}$  is a combination of several effects, besides the mentioned main effect  
 300 on  $y_{\text{O}_2,IVC}$ . According to Molina [22], the EGR rate affects the adiabatic coefficient  $\gamma$   
 301 decreasing its value [40], which is a term of equation (3) used for the calculation of  $T_{ub}$ ;  
 302 both effects are reflected on equation (4).

#### 303 4. Model correction based on $\text{NO}_X$ reduction mechanism

304 Although most of the predictive  $\text{NO}_X$  models only take into account the  $\text{NO}_X$  forma-  
 305 tion mechanism, if the  $\text{NO}_X$  reduction mechanism in the flame is considered the accuracy  
 306 of the basic model presented in the previous section can be improved. According to the  
 307 diesel diffusion flame model proposed by Dec [41], the local conditions inside of a quasi-  
 308 steady diffusion flame (a region with high temperatures not far from the adiabatic flame  
 309 temperature, and a mixture of both burned and cracked fuel gases) correspond to an even  
 310 more reducing atmosphere than that in the re-burning zone of a thermal power plant,  
 311 where an important  $\text{NO}_X$  reduction rate is achieved [42, 43]. Taking into account this  
 312 effect, a  $\text{NO}_X$  reduction model is proposed. The model considers that the  $\text{NO}_X$  going  
 313 through the reacting spray cone from two possible sources:

- 314 1. From exhaust gases in the combustion chamber coming from internal (residual  
 315 gases) or external EGR.
- 316 2. The  $\text{NO}_X$  produced in the current combustion that can be re-entrained into the  
 317 reduction zone of the flame.

318 When the  $\text{NO}_X$  molecules are entrained in the spray, the model considers that they  
 319 go through the reductive atmosphere existing inside the diffusion flame and part of them  
 320 are reduced thus disappearing [44]. The percentage of disappearance depends on the  
 321 local temperature and composition as well as on the residence time, and it is strongly  
 322 linked to the mixing rate of the combustion products [45].

323 The complete formation and reduction process is represented in Figure 8. Appendix A  
 324 provides details of  $\text{NO}_X$  reduction mechanism formulation that allows to derive the  
 325 following equation:

$$y_{\text{NO}_X,exh} = \frac{m_{\text{NO}_X,comb} \cdot (1 - K_{re} \cdot Fr \cdot \varepsilon)}{m_a + m_f + m_{EGR} \cdot Fr \cdot \varepsilon} \quad (7)$$

326 where  $y_{\text{NO}_X,exh}$  stands for the  $\text{NO}_X$  mass fraction at the exhaust,  $m_{\text{NO}_X,comb}$  is the  
 327  $\text{NO}_X$  mass produced at the current combustion,  $m_a$ ,  $m_f$  and  $m_{EGR}$  are the fresh air,  
 328 fuel and EGR mass respectively,  $Fr$  is the fuel-air equivalence ratio,  $K_{re}$  is the fraction  
 329 of gas re-entrained (0.5 used here, see Appendix A), and  $\varepsilon$  is the efficiency of the  $\text{NO}_X$   
 330 reduction (1 used here, see Appendix A).

331 Taking into account the effect of the  $\text{NO}_X$  reduction mechanism, the net  $\text{NO}_X$  emitted  
 332 in each cycle can be expressed as follows:

$$m_{\text{NO}_X,re} = y_{\text{NO}_X,exh} \cdot (m_a + m_f) \quad (8)$$

333 where  $m_{\text{NO}_X,re}$  is the net  $\text{NO}_X$  emitted considering re-burning, and  $y_{\text{NO}_X,exh}$  is cal-  
 334 culated with equation (7), where it is assumed that  $m_{\text{NO}_X,comb} = m_{\text{NO}_X,base}$ , calculated  
 335 with equation (1).

336 The constants  $K_1$ ,  $K_2$  and  $K_3$  (used for the  $y_{\text{NO}_X,exh}$  calculation) were fitted again  
 337 using the training operating points used for the base model in section 3.3. Figure 9 shows  
 338 the measured and predicted values before and after the re-burning correction (top), and  
 339 the corresponding relative error when varying EGR rate (from 0% to 32%) at 2500 rpm  
 340 and 45% load. As it can be noticed, the prediction error is slightly reduced for all the  
 341 cases. In the rest of operating points (not shown) this trend is also followed. Compared

342 with the results obtained in section 3.3, the mean relative error of the global study is  
 343 improved about 1.3% by the  $\text{NO}_X$  reduction mechanism correction.

## 344 5. Empirical correction

345 According to section 3.3 the model coefficient  $K_3$  is quite constant, while impor-  
 346 tant variations are obtained in the two other model coefficients. As an intermediate  
 347 step between the local and global approach for the model fitting, tabulated values for  
 348  $K_1 (n/2000)^{K_2}$  while a global value for  $K_3$  will now be used. This is a way of profiting  
 349 the high repeatability found in constant  $K_3$  of the model while keeping the flexibility  
 350 of the local fitting approach for adapting to different operating conditions. Next it will  
 351 be proved that using local  $K_1$  and  $K_2$  is equivalent of normalising the  $\text{NO}_X$  production  
 352 with a nominal operating condition:

$$m_{\text{NO}_X} = m_{\text{NO}_X,0} \frac{m_{\text{NO}_X, re}}{m_{\text{NO}_X, re,0}} \quad (9)$$

353 where  $m_{\text{NO}_X,0}$  is the  $\text{NO}_X$  production at the reference operating conditions, and  $m_{\text{NO}_X, re}$   
 354 is the prediction delivered by the model described in the previous section (which depends  
 355 on the actual measurements, including the in-cylinder pressure).  $m_{\text{NO}_X, re,0}$  stands for  
 356 the model prediction at the nominal conditions (which can be calculated beforehand).

357 For the present work nominal conditions are selected as those with nominal settings  
 358 (according to ECU calibration) at the considered engine speed and load. According  
 359 to the usual control algorithms, that means that the reference situation has the same  
 360 injection settings (number and disposition of injections, rail pressure control reference)  
 361 than the actual operating point, and the model only has to compensate the deviations  
 362 in the air loop or working temperature, what is consistent with the assumptions made  
 363 on the experimental plan in section 2.

364 Combining expression (9) with the model according to equation (1), (7) and (8), and  
 365 considering that the terms depending on  $K_1$  and  $K_2$  in equation (1) are cancelled because  
 366 both the reference point and the considered conditions share the same engine speed and  
 367 constants, equation (9) can be written as:

$$m_{\text{NO}_X} = m_{\text{NO}_X,0} \cdot \frac{(A \cdot B_0)}{(A_0 \cdot B)} \quad (10)$$

368 with:

$$369 \quad A = \left( \int_{\alpha} dQ_b(\alpha) \cdot e^{\left(\frac{K_3}{T_{ad}(\alpha)}\right)} d\alpha \right) \cdot \left( 1 - K_{re} \cdot \left( \frac{m_a}{m_f} \right) \cdot \varepsilon \right) \cdot (m_a + m_f)$$

370 being the  $\text{NO}_X$  mass predicted by the model at the current operating conditions, and  
 371  $A_0$  the equivalent term at the nominal conditions. And

$$372 \quad B = m_a + m_f + m_{EGR} \cdot \left( \frac{m_f}{m_a} \right) \cdot \varepsilon$$

373 is a mass term affected by the reduction constant  $\varepsilon$  at the considered operating con-  
 374 ditions, and  $B_0$  at the reference conditions. Note that the ratio  $m_{\text{NO}_X,0} \cdot B_0/A_0$  can  
 375 be precomputed and stored according to a look-up table approach. Hence in the final  
 376 model only  $A$  (derived from  $T_{ad}$  and  $dQ_b$  evolutions) and  $B$  (derived from mean variables  
 377 obtained from the ECU) are calculated and used for correcting the tabulated value.

378 Note that equation (10) implies to assume that the model proposed in the previous  
 379 section is able to correctly predict the variations with respect to the reference point when  
 380 the EGR rate,  $p_{itk}$  or  $T_{itk}$  are changed, but it cancels any bias error in the reference  
 381 point because the model, according to expression (9), would result in  $m_{NO_X,exp_0}$  for the  
 382 reference conditions. This fact is demonstrated in Figure 10, where the original model  
 383 and the one using the reference condition are compared. The later property can be also  
 384 used for engine diagnosis: the deviation of the predicted  $NO_X$  value, with respect to the  
 385 experimental value at the reference operating point, is an estimation of the degradation  
 386 of the engine (e.g. when it is new and after several thousands of hours of operation).

387 Besides the accuracy improvement, it is interesting to note that the empirical correc-  
 388 tion leads to have only one model constant  $K_3$ , thus acquiring a higher robustness. Note  
 389 that according to Figure 6 only the estimate of  $K_3$  was shown to be consistent along  
 390 the whole engine operation range. A value of  $K_3 = -48767$  was fitted using the training  
 391 operating points used for the previous model fittings (which slightly differs from the value  
 392 shown in Figure 6 because now the re-burning correction is considered). Figure 11 shows  
 393 an scatter plot of the prediction obtained for all the data set, including both training and  
 394 validation sets; error metrics are summarised in Table 3 which are consistently better  
 395 than those exhibited by the global fitting approach.

## 396 6. Model validation

397 As stated, the model was fitted exclusively using the training data set that was  
 398 constructed according to the second column of Table 2. This tests matrix corresponds  
 399 to partial load tests at several engine speeds. It is important to emphasise that the  
 400 engine speed for the model fitting only reaches up to 3000 rpm; this was done because  
 401 the main objective for the model development was the EGR zone, restricted to engine  
 402 speeds below 3100 rpm. However, the validation data set covers the complete engine  
 403 map, including operating points at 3500 and 4000 rpm in a wide range of loads, even full  
 404 load tests. Hence the validation covers significant extrapolations of the engine operating  
 405 range (although the bias is corrected thanks to the empirical correction).

406 The complete matrix is detailed in the third column of Table 2 and characteristics of  
 407 the applied variations in EGR,  $p_{itk}$  and  $T_{itk}$  are shown in Figure 2. At operating points  
 408 in which there is no EGR in the original settings, no EGR variation was performed, but  
 409  $p_{itk}$  and  $T_{itk}$  variations were tested. In all cases, the reference conditions for the final  
 410 model were those of the original ECU calibration.

411 The grey points in Figure 11 correspond to the measured and predicted  $NO_X$  values  
 412 for the validation data set, including all variations in EGR,  $p_{itk}$  and  $T_{itk}$ . As can be seen,  
 413 the model keeps its linear trend in the complete range of tests. The prediction errors are  
 414 summarised in last row of Table 3, which do not importantly differ of those obtained in  
 415 the model fitting. Although the model has been extrapolated (validation tests are out of  
 416 the training data set range), the use of an empirical correction based on the measured  
 417  $NO_x$  at the reference conditions made possible to avoid great errors.

## 418 7. Computational issues

419 As previously stated, an important issue for control applications is the calculation  
 420 time. The simplified combustion diagnostic code that feeds the model takes 2.5 ms to



421 calculate  $dQ_b$  using a crank-angle step of  $0.2^\circ$ . With the algorithm proposed in section  
 422 3.2,  $T_{ad}$  can be calculated in 1.1 ms plus. The calculation time of the  $\text{NO}_X$  model is  
 423 0.9 ms in a 3 GHz PC using a Matlab code, thus the total calculation time of the final  
 424 model is about 4.5 ms. Table 4 summarises the total calculation times and errors (for  
 425 the parametric study varying EGR rate) using the 3 methods stated in section 3.1 for  
 426 the heat release estimate: the original model [9] with fast heat release calculation and no  
 427 corrections (method 1), the complete diagnosis code with all the submodels proposed in  
 428 [32] (method 2) and the optimized heat release calculation with the corrections (method  
 429 3). The data acquisition time, about 4.5 ms plus, has not been included in the total  
 430 calculation time in any case.

431 Considering the results obtained with the different methods, it can be concluded that  
 432 the proposed model is slightly slower than the fast method but it increases importantly  
 433 the final accuracy. In any case, as the total calculation time is smaller than an engine  
 434 cycle, method 3 is considered fast enough for being computed on a real-time approach  
 435 and to handle with transients test. In comparison with similar  $\text{NO}_X$  models [3, 8, 16]  
 436 the proposal is faster (1 s, 0.5 s and 0.1 s respectively), probably because these other  
 437 models are not optimised in this aspect, as Hountalas *et al.* [16] recognize in their  
 438 work. Moreover, the calculation time of these models is comparable to that of method  
 439 2 where the heat release calculation algorithm was the starting point for the optimised  
 440 heat release calculation. Regarding the accuracy, the proposed model has a global mean  
 441 error of about 15%, lower than the 23% of Egnell *et al.* proposal [3] and in the order of  
 442 the one of Andersson *et al.* [8], although the direct comparison is difficult because they  
 443 are considering different engines and operating conditions.

## 444 8. Conclusions

445 A control oriented model for raw  $\text{NO}_X$  emission has been presented. The main  
 446 model inputs are the in-cylinder pressure evolution and other operative variables that  
 447 are commonly available in any automotive ECU (air mass flow, injected fuel mass, etc.).  
 448 The in-cylinder pressure signal is used for tracking the  $\text{NO}_X$  formation through the  
 449 thermal mechanism, on the basis of the flame temperature estimation.  $\text{NO}_X$  reduction  
 450 through the re-burning process is also considered. Finally, the model is used for providing  
 451 a local correction to the tabulated  $\text{NO}_X$  produced at a given engine load and speed.

452 The model has proved its capability to properly predict the effect of variations in  
 453 the intake mix composition (EGR rate), boost pressure and intake temperature, on the  
 454  $\text{NO}_X$  production; the extrapolation of the model beyond its fitting range has proven its  
 455 robustness.

456 Concerning the calculation time, it was optimized by proposing simplified sub-models  
 457 to calculate  $dQ_b$  and  $T_{ad}$  in about 3.5 ms per engine cycle, plus 1 ms to compute the  
 458  $\text{NO}_X$  emissions. This calculation time is suitable for real time applications.

459 **References**

- 460 [1] J. Arregle, J.J. López, C. Guardiola and C. Monin, On board NO<sub>x</sub> prediction in diesel engines:  
461 A physical approach, in *Automotive Model Predictive Control: Models, Methods and Applications*  
462 (*Lecture Notes in Control and Information Sciences*), Berlin:Springer (2010).
- 463 [2] R. Moos, A brief overview on automotive exhaust gas sensors based on electroceramics, *Int. J. Appl.*  
464 *Ceram. Technol.* 2 (2005) 401–413.
- 465 [3] R. Egnell, Combustion Diagnostics by Means of Multizone Heat Release Analysis and NO Calculation,  
466 SAE Paper 981424 (1998).
- 467 [4] D.J. Timoney, J.M. Desantes, L. Hernández and C.M. Lyons, The development of a semi-empirical  
468 model for rapid NO<sub>x</sub> concentration evaluation using measured in-cylinder pressure in diesel engines,  
469 *Proc. Inst. Mech. Eng. Part D-J. Automob. Eng.* 219 (2005) 621–631.
- 470 [5] D. Cipolat, Analysis of energy release and NO<sub>x</sub> emissions of a CI engine fuelled on diesel and DME,  
471 *Appl. Therm. Eng.* 27 (2007) 2095–2103.
- 472 [6] J.J. Hernández, J. Pérez-Collado and J. Sanz-Argent, Role of the Chemical Kinetics on Modeling  
473 NO<sub>x</sub> Emission in diesel Engines. *Energy & Fuels* 22 (2008) 262–272.
- 474 [7] M. Hirsch, K. Oppenauer, and L. del Re, Dynamic engine emission models, in *Automotive Model*  
475 *Predictive Control: Models, Methods and Applications (Lecture Notes in Control and Information*  
476 *Sciences)*, Berlin:Springer (2010).
- 477 [8] M. Andersson, B. Johansson, A. Hultqvist and C. Noehre, A Predictive Real Time NO<sub>x</sub> Model for  
478 Conventional and Partially Premixed diesel Combustion, SAE Paper 2006-01-3329 (2006).
- 479 [9] J. Arregle, J.J. López, C. Guardiola and C. Monin, Sensitivity Study of a NO<sub>x</sub> Estimation model  
480 for On-Board Applications, SAE Paper 2008-01-0640 (2008).
- 481 [10] J.M. Desantes, J. Galindo, C. Guardiola, V. Dolz, Air mass flow estimation in turbocharged diesel  
482 engines from in-cylinder pressure measurement, *Exp. Therm. Fluid Sci.* 34 (2010) 37–47.
- 483 [11] J.M. Luján, V. Bermúdez, C. Guardiola, A. Abbad, A methodology for combustion detection in  
484 diesel engine through in-cylinder pressure derivative signal, *Mech. Syst. Signal Pr.* (2010),  
485 doi:10.1016/j.ymsp.2009.12.012.
- 486 [12] S. Leonhardt, N. Müller, R. Isermann, Methods for engine supervision and control based on cylinder  
487 pressure information, *IEEE/ASME Transactions on mechatronic* 4 (1999) 235–245.
- 488 [13] M. Hasegawa, Y. Shimasaki, S. Yamaguchi, M. Kobayashi, M. Sakamoto, N. Kitayama, T. Kanda,  
489 Study on ignition timing control for diesel engines using in-cylinder pressure sensor, SAE paper  
490 2006-01-0180 (2006).
- 491 [14] Y. Shimasaki, M. Kobayashi, H. Sakamoto, M. Ueno, M. Hasegawa, S. Yamaguchi, T. Suzuki,  
492 Study on engine management system using chamber pressure sensor integrated with spark plug,  
493 SAE Paper 2004-01-0519 (2004).
- 494 [15] F. Payri, A. Broatch, B. Tormos, V. Marant, New methodology for in-cylinder pressure analysis  
495 in direct injection diesel engines - application to combustion noise, *Meas. Sci. Technol.* 16 (2005)  
496 540–547.
- 497 [16] D.T. Hountalas, N. Savva and R.G. Papagiannakis, Development of a New Physically Based  
498 Semi-empirical NO<sub>x</sub> Model Using the measured Cylinder Pressure, THIESEL 2010 Conference  
499 on Thermo- and Fluid Dynamic Processes in Diesel Engines (2010).
- 500 [17] M. Devarakonda, G. Parker, J.H. Johnson and V. Strots, Model-based control system design in  
501 a urea-SCR aftertreatment system based on NH<sub>3</sub> sensor feedback, *Int. J. Automot. Technol.* 10  
502 (2009) 653–662.
- 503 [18] S.R. Katare, J. E. Patterson and P. M. Laing, Diesel Aftertreatment Modeling: A Systems Approach  
504 to NO<sub>x</sub> Control, *Ind. Eng. Chem. Res* 46 (2007) 2445–2454.
- 505 [19] J. Galindo, H. Climent, C. Guardiola, A. Tiseira and J. Portalier, Assessment of a sequentially  
506 turbocharged diesel engine on real-life driving cycles, *Int. J. Vehicle Design* 49 (2009) 214–234.
- 507 [20] J. Tichy, G. Gautschi, *Piezoelektrische Messtechnik*, Springer Verlag, Berlin, 1980.
- 508 [21] N. Ladommatos, S. Abdelhalim and H. Zhao, Control of oxides of nitrogen from diesel engines  
509 using diluents while minimising the impact on particulate pollutants, *Appl. Therm. Eng.* 18 (1998)  
510 963–980.
- 511 [22] S. Molina, Influencia de los parámetros de inyección y la recirculación de gases de escape sobre el  
512 proceso de combustión en un motor diesel, Editorial Reverté, Barcelona, 2005.
- 513 [23] Y.A Zeldovich, The Oxidation of Nitrogen in Combustion and Explosions, *Acta Physicochim. USSR*  
514 21 (1946) 577–628.
- 515 [24] C.P. Fenimore, Formation of Nitric Oxide in Premixed Hydrocarbon Flames, 13<sup>th</sup> Symposium  
516 International of Combustion (1971) 373–379.

- 517 [25] M. Ghazikhani, M.E.Feyz, A.Joharchi, Experimental investigation of the Exhaust Gas Recirculation  
518 effects on irreversibility and Brake Specific Fuel Consumption of indirect injection diesel engines,  
519 Appl .Therm. Eng. 30 (2010) 1711–1718.
- 520 [26] C. Schwerdt. Modeling NO<sub>x</sub>-Formation in Combustion Processes. MSc Thesis. Department of Au-  
521 tomatic Control. Lund University. Sweden.
- 522 [27] T.T. AL-Shemmer, S. Oberweis, Correlation of the NO<sub>x</sub> emission and exhaust gas temperature for  
523 biodiesel, Appl .Therm. Eng. 31 (2011) 1682–1688.
- 524 [28] F. Chmela, M. Engelmayer, G. Pirker and A. Wimmer, Prediction of Turbulence Controlled Com-  
525 bustion in diesel Engines, THIESEL 2004 Conference on Thermo-and Fluid Dynamic Processes in  
526 diesel Engines Valencia (2004).
- 527 [29] A. Uludogan, D.E. Forester and R.D. Reitz, Modelling the Effect of Engine Speed on the Combustion  
528 process and Emissions from diesel Engines, SAE Paper 962056 (1996).
- 529 [30] J. B. Heywood, Internal Combustion Engine Fundamentals, McGraw-Hill, New York, USA, 1988.
- 530 [31] M.F.J. Brunt, H. Rai and A.L. Emtage, Calculation of Heat Release Energy from Engine Cylinder  
531 Pressure Data, SAE Paper 981052 (1998). Appl. Therm. Eng. 26 (2006) 226–236.
- 532 [32] F. Payri, S. Molina, J. Martín, O. Armas Influence of measurement errors and estimated parameters  
533 on combustion diagnosis. Appl. Therm. Eng. 26 (2006) 226–236.
- 534 [33] J.R. Serrano, F.J. Arnau, V. Dolz, P. Piqueras Methodology for characterisation and simulation of  
535 turbocharged diesel engines combustion during transient operation. Part 1: Data acquisition and  
536 post-processing. Appl. Therm. Eng. 29 (2009) 142–149.
- 537 [34] J.R. Serrano, F.J. Arnau, V. Dolz, P. Piqueras Methodology for characterisation and simulation of  
538 turbocharged diesel engines combustion during transient operation. Part 2: Phenomenological  
539 combustion simulation. Appl. Therm. Eng. 29 (2009) 150–158
- 540 [35] G. Woschni. A universally applicable equation for the instantaneous heat transfer coefficient in the  
541 internal combustion engine. SAE paper 670931 (1967).
- 542 [36] G. Woschni. Die Berechnung der Wandverluste und der thermischen Belastung der Bauteile von  
543 dieselmotoren. MTZ 31/12 (1970) 491–499.
- 544 [37] M. Lapuerta, O. Armas, J.J. Hernández. Diagnosis of DI diesel combustion from in-cylinder pressure  
545 signal by estimation of mean thermodynamic properties of the gas, Appl. Therm. Eng. 19 (1999)  
546 513–529.
- 547 [38] P.K. Senecal, J. Xin and R.D. Reitz, Prediction of Residual Gas Fraction in IC Engines, SAE Paper  
548 962052 (1996).
- 549 [39] Md. Nurun Nabi, Theoretical investigation of engine thermal efficiency, adiabatic flame temperature,  
550 NO<sub>x</sub> emission and combustion-related parameters for different oxygenated fuels, Appl. Therm. Eng.  
551 30 (2010) 839–844.
- 552 [40] F. Payri, M. Lapuerta, P. Cazaux, Insight into combustion process of a diesel engine with exhaust  
553 gas recirculation, SIA paper 9506A13 (1995).
- 554 [41] J.E. Dec, A Conceptual Model of DI diesel Combustion Based on Laser-sheet Imaging, SAE Paper  
555 970873 (1997).
- 556 [42] E. Chaize, D.E. Webster, B. Krutzsch, G. Wenninger, M. Weibel, Sh. Hodjati, C. Petit, V. Pitchon,  
557 A. Kiennemann, R. Loenders, O. Monticelli, P.A. Jacobs, J.A. Martens and B. Kasemo, Reduction  
558 of NO<sub>x</sub> in Lean Exhaust by Selective NO<sub>x</sub>-Recirculation (SNR-Technique) Part II: NO<sub>x</sub> Storage  
559 Materials, SAE Paper 982593 (1998).
- 560 [43] B. Krutzsch, G. Wenninger, M.Weibel, P.Stapf, A.Funk, D.E. Webster, E.Chaize, B. Kasemo, J.A.  
561 Martens, A Kiennemann, Reduction of NO<sub>x</sub> in Lean Exhaustby Selective NO<sub>x</sub>-Recirculation (SNR  
562 Technique)- part I: System and Decomposition Process, SAE Paper 982592 (1998).
- 563 [44] R. Vellaisamy, N. N Clark, G.J. Thompson, R.J. Atkinson, C.A. Tissera, M.M. Swartz, Assessment  
564 of NO<sub>x</sub> Destructions in Diesel Engines by Injecting NO in the Intake Manifold, SAE Paper 2005-  
565 01-0370 (2005).
- 566 [45] F. Payri, J.Arregle, J.J López and E. Mocholí, Diesel NO<sub>x</sub> Modeling with a Reduction Mechanism  
567 for the Initial NO<sub>x</sub> Coming from EGR or Re-entrained Burned Gases, SAE Paper 2008-01-1188  
568 (2008).

**List of figures**

569  
570  
571  
572  
573  
574  
575  
576  
577  
578  
579  
580  
581  
582  
583  
584  
585  
586  
587  
588  
589  
590  
591  
592  
593  
594  
595  
596

Figure 1. Test cell scheme.

Figure 2. Range of the main variables involved in the experimental design. The range of NO<sub>x</sub> variation can be checked in Figure 11.

Figure 3. Structure of the main cycle in the combustion diagnosis code.

Figure 4. Adiabatic flame temperature calculation scheme.

Figure 5. Temperature evolution during the combustion process at the following operating point: speed 2500 rpm, 58% load, 19.2% EGR.

Figure 6. Optimal value of the model constants for a local optimisation (marks) and a global optimisation (dashed line).

Figure 7. Base model NO<sub>x</sub> prediction varying EGR rate, boost pressure and inter-cooler temperature, at 2000 rpm at low and high load operating points.

Figure 8. Theoretical re-burning scheme.

Figure 9. NO<sub>x</sub> modeled with and w/o re-burning effect at 2500 rpm and 58% load.

Figure 10. Modelled vs. measured NO<sub>x</sub> on four selected operating conditions.

Figure 11: Model prediction with all improvements applied.

597 **Appendix A. NO<sub>X</sub> reduction mechanism calculation**

598 *Appendix A.1. Reduction of the NO<sub>X</sub> coming from the EGR*

599 If it is assumed that the NO<sub>X</sub> mass fraction at the exhaust ( $y_{NO_X,exh}$ ) remains  
600 invariable between exhaust and EGR, the NO<sub>X</sub> mass re-entrained is:

$$m_{EGR} \cdot y_{NO_X,exh} \quad (A.1)$$

601 The NO<sub>X</sub> mass that takes part in the combustion process is then:

$$m_{EGR} \cdot y_{NO_X,exh} \cdot F_r \quad (A.2)$$

602 Assuming a reduction efficiency ( $\varepsilon$ ), the NO<sub>X</sub> mass diminution is:

$$m_{EGR} \cdot y_{NO_X,exh} \cdot F_r \cdot \varepsilon \quad (A.3)$$

603 where  $\varepsilon=1$ , considering that the 100% of the re-entrained NO<sub>X</sub> is destroyed.

604  
605 The net NO<sub>X</sub> mass per cycle that exits from the cylinder is:

$$\begin{aligned} m_{exh} \cdot y_{NO_X,exh} &= m_{NO_Xnet} + m_{EGR} \cdot y_{NO_X,exh} \cdot (1 - F_r \cdot \varepsilon) \\ m_{NO_Xnet} &= y_{NO_X,exh} \cdot (m_{exh} - m_{EGR} \cdot (1 - F_r \cdot \varepsilon)) \\ &= y_{NO_X,exh} \cdot (m_a + m_f + m_{EGR} - m_{EGR} \cdot (1 - F_r \cdot \varepsilon)) \\ &= y_{NO_X,exh} \cdot (m_a + m_f + m_{EGR} \cdot F_r \cdot \varepsilon) \end{aligned} \quad (A.4)$$

606 where,  $m_{NO_Xnet}$  is the net NO<sub>X</sub> produced in the current combustion and  $m_{exh}$  is the  
607 gas mass per cycle that exits from the cylinder.

608 Then the following expression can be obtained:

$$y_{NO_X,exh} = \frac{m_{NO_Xnet}}{m_a + m_f + m_{EGR} \cdot F_r \cdot \varepsilon} \quad (A.5)$$

611 *Appendix A.2. Reduction of the NO<sub>X</sub> produced during the combustion process*

612 Thanks to the NO<sub>X</sub> reduction mechanism, a part of the NO<sub>X</sub> mass produced at the  
613 current combustion ( $m_{NO_Xcomb}$ ) will be re-entrained, and hence the net NO<sub>X</sub> produced  
614 at the current cycle ( $m_{NO_Xnet}$ ) will be lower. Based on this fact, the following situations  
615 can be considered:

- 616 1. At the start of combustion (SOC): the efficiency of the NO<sub>X</sub> reduction is 0 (none  
617 NO<sub>X</sub> has been re-entrained).
- 618 2. At the end of combustion (EOC): if it is assumed that all the combustion products  
619 are homogeneously mixed in the chamber, the efficiency will be  $F_r$ .

620 In order to consider all the combustion evolution it is assumed the intermediate sit-  
621 uation:  $K_{re} \cdot F_r$ , where  $K_{re} = 0.5$ .

622

623 Taking into account the efficiency  $\varepsilon$  of the  $\text{NO}_X$  reduction mechanism (in this case  
 624 related to the  $\text{NO}_X$  produced and re-entrained), the following expression is obtained:

$$m_{\text{NO}_X\text{net}} = m_{\text{NO}_X\text{comb}} \cdot (1 - K_{re} \cdot F_r \cdot \varepsilon) \quad (\text{A.6})$$

625 Therefore, the relationship between  $m_{\text{NO}_X\text{comb}}$  and  $y_{\text{NO}_X,\text{exh}}$  is:

$$y_{\text{NO}_X,\text{exh}} = \frac{m_{\text{NO}_X\text{comb}} \cdot (1 - K_{re} \cdot F_r \cdot \varepsilon)}{m_a + m_f + m_{\text{EGR}} \cdot F_r \cdot \varepsilon} \quad (\text{A.7})$$

	Dimension	Units
Bore	85	[mm]
Stroke	96	[mm]
Unitary piston displacement	545.75	[ $cm^3$ ]
Connecting rod length	152	[mm]
Compression ratio	17:1	[-]

Table 1: Engine characteristics.

Speed [rpm]	Model development [Load %]	Model validation [Load %]
780	idle	-
1000	35, 55	70, Full load
1500	30, 45	10, 75
2000	15, 45, 58	25, 65, Full load
2500	35, 45, 58	15, 75
2850	20, 40	55, Full load
3000	15	40, 70, Full load
3500	-	10, 20, 40, 70, Full load
4000	-	15, 40, 70, Full load

Table 2: Operating points used for development and validation of the model.

	Mean absolute error [mg/str]		Mean relative error [%]	
	Training data	Validation data	Training data	Validation data
$K_{1,2,3}$ <i>Local fitting</i>	0.0489	0.2296	14.48	15.83
$K_{1,2,3}$ <i>Global fitting</i>	0.0499	0.3173	17.96	18.39
$K_3$ <i>Global+corrected</i>	0.0421	0.2163	15.12	17.71

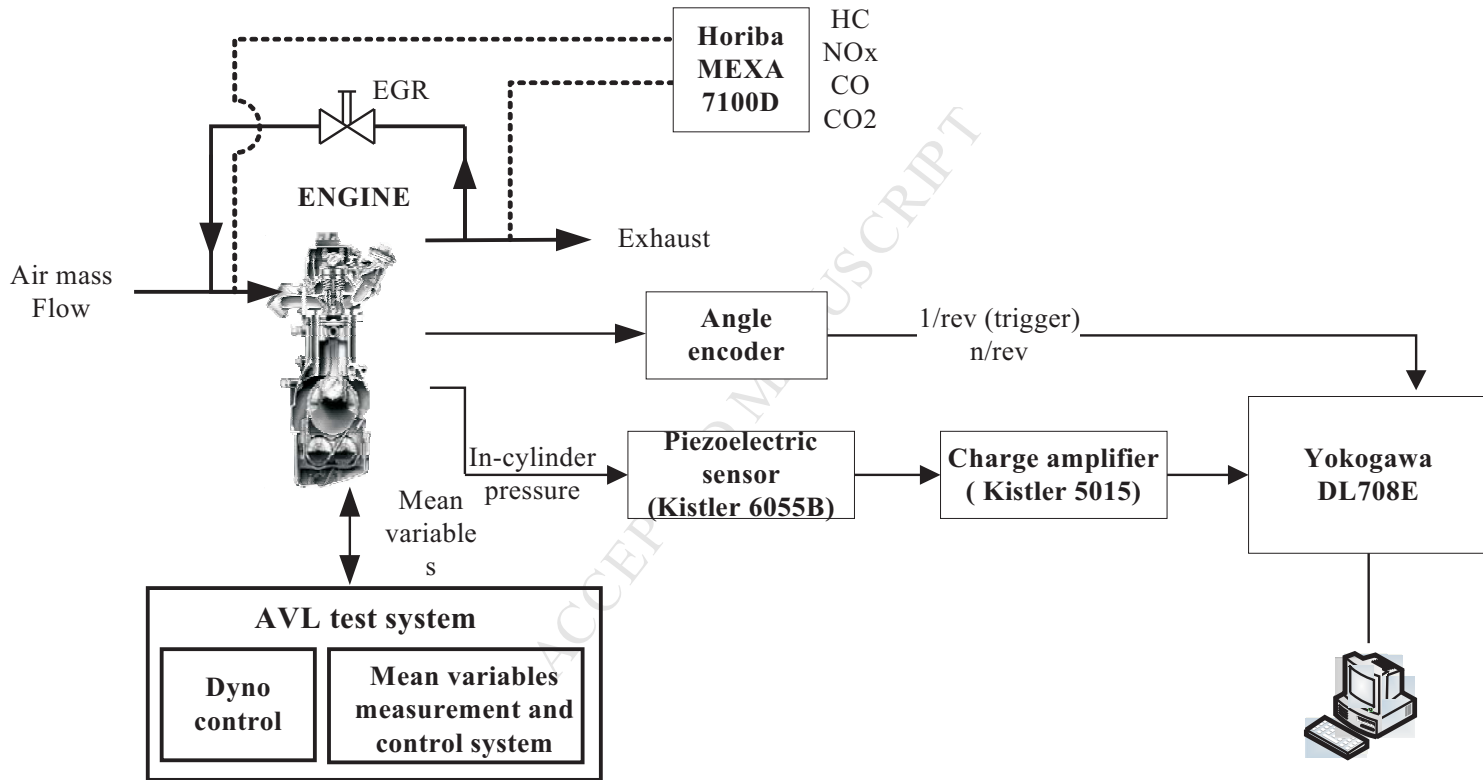
Table 3: Model fitting mean errors.

	Combustion diagnostic		
	Fast $dQ_b$	Complete	Simplified
Calculation time [ms]	4	487	4.5
Relative error [%]	15.6	9.5	10.2

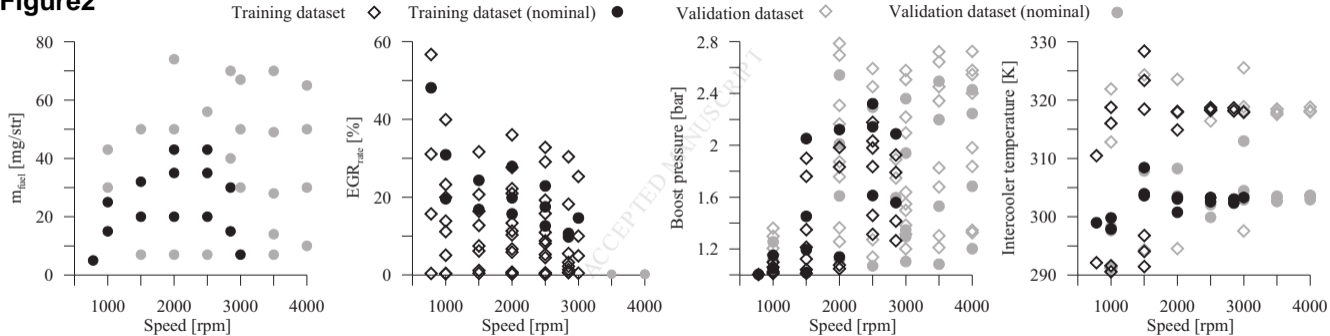
Table 4: Calculation time and accuracy of the model using different methods to calculate  $dQ_b$ .

Figure1

Gas Analyzer





**Figure 2**

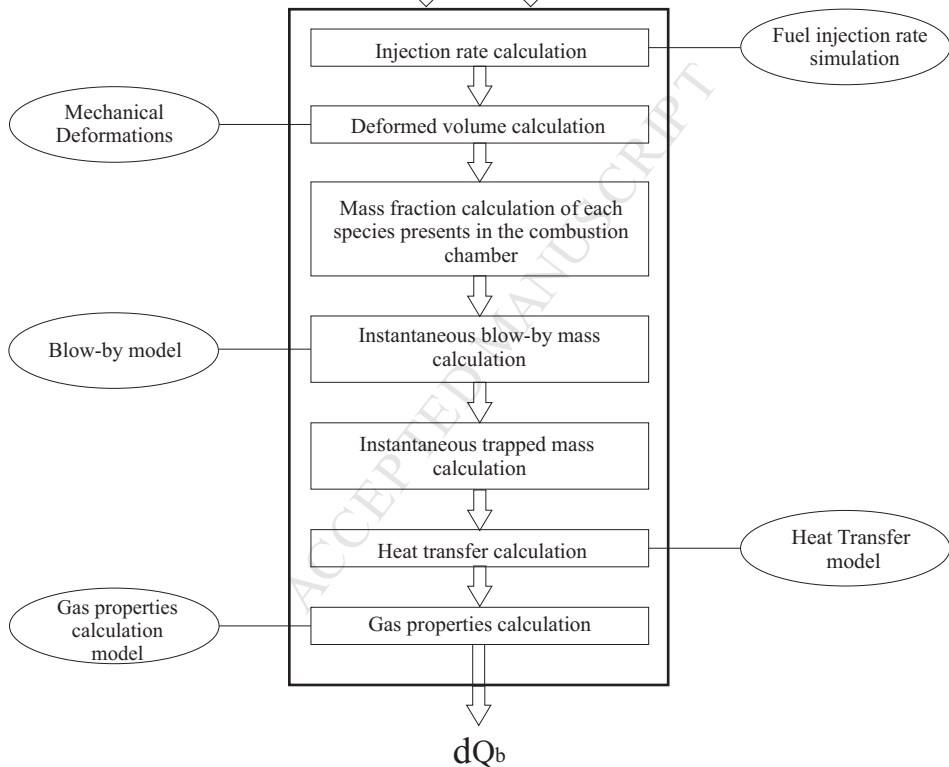
**Figure3****Pcyl( $\alpha$ )**      **Mean Variables**

Figure 4

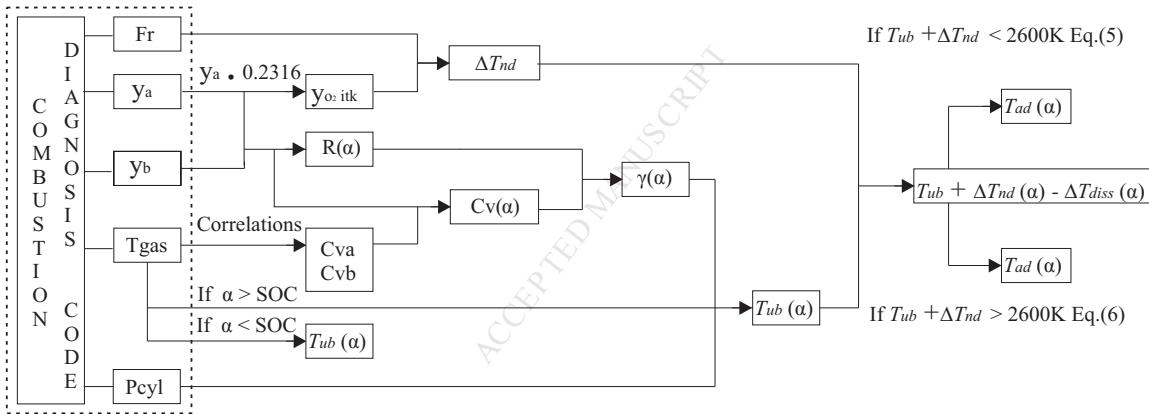


Figure 5

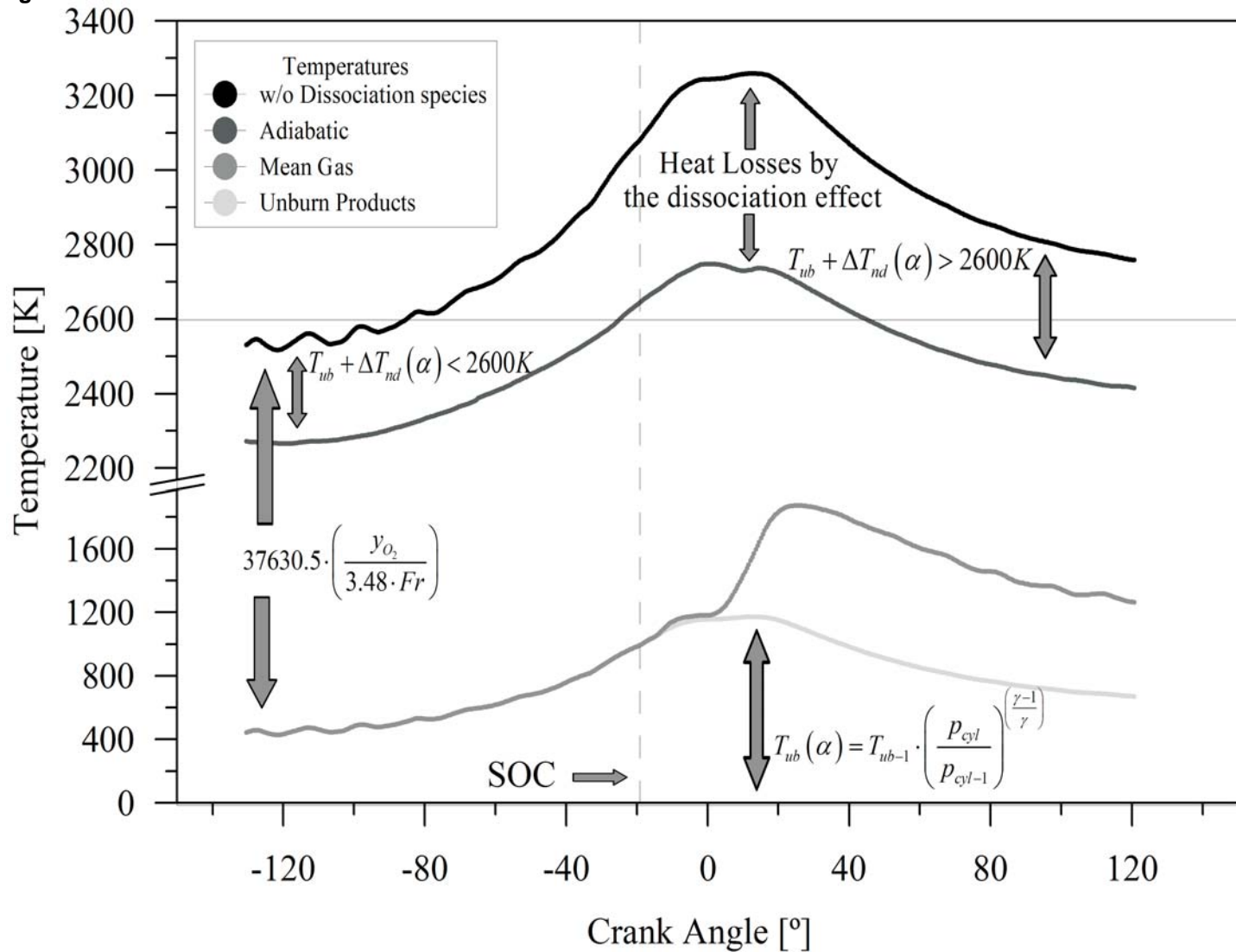


Figure6

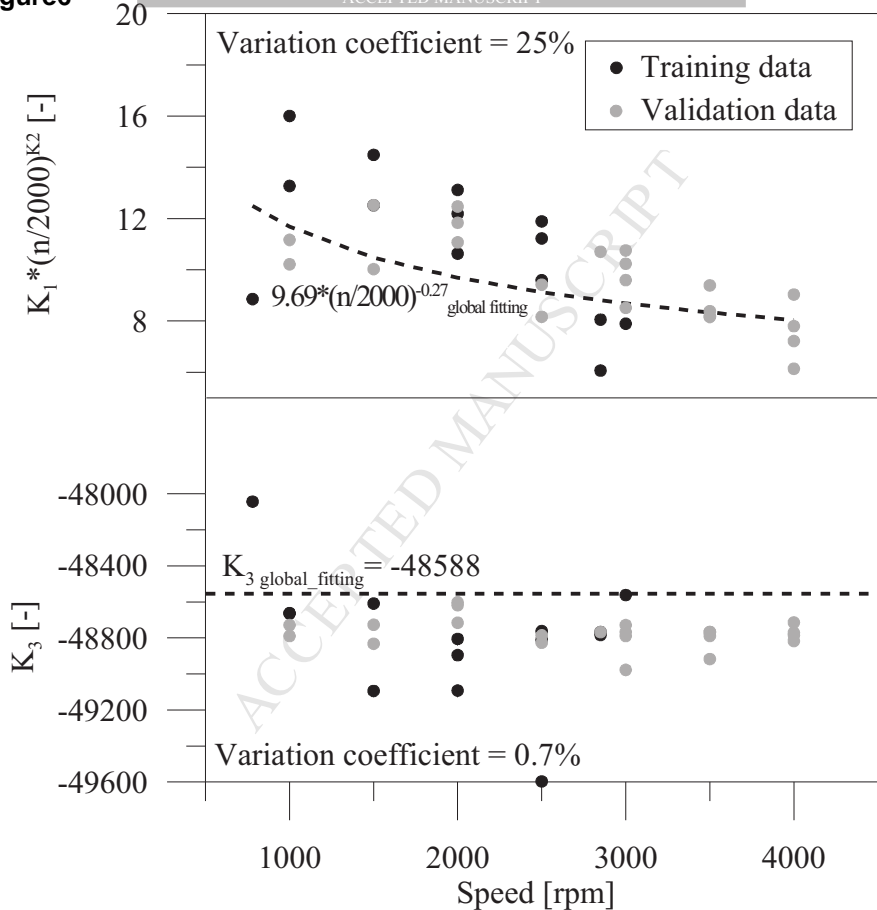
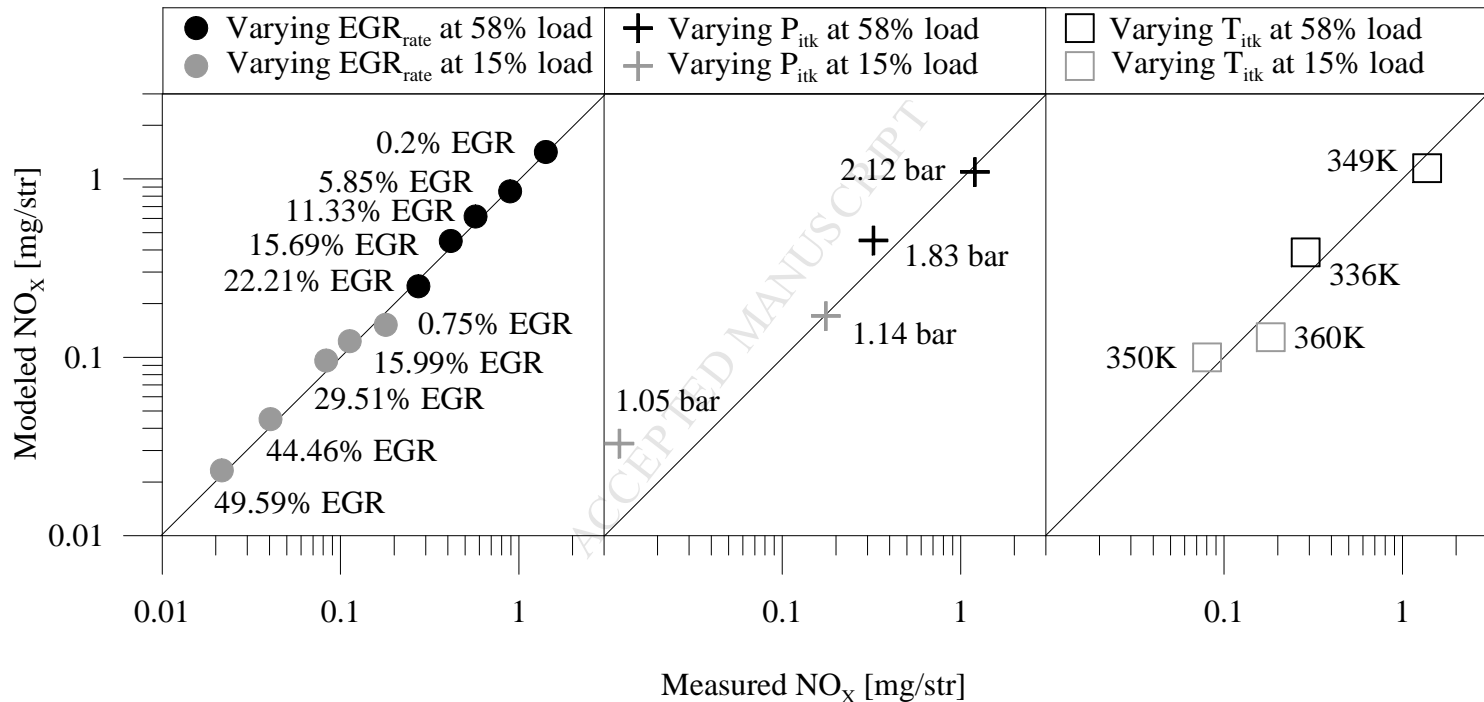


Figure7



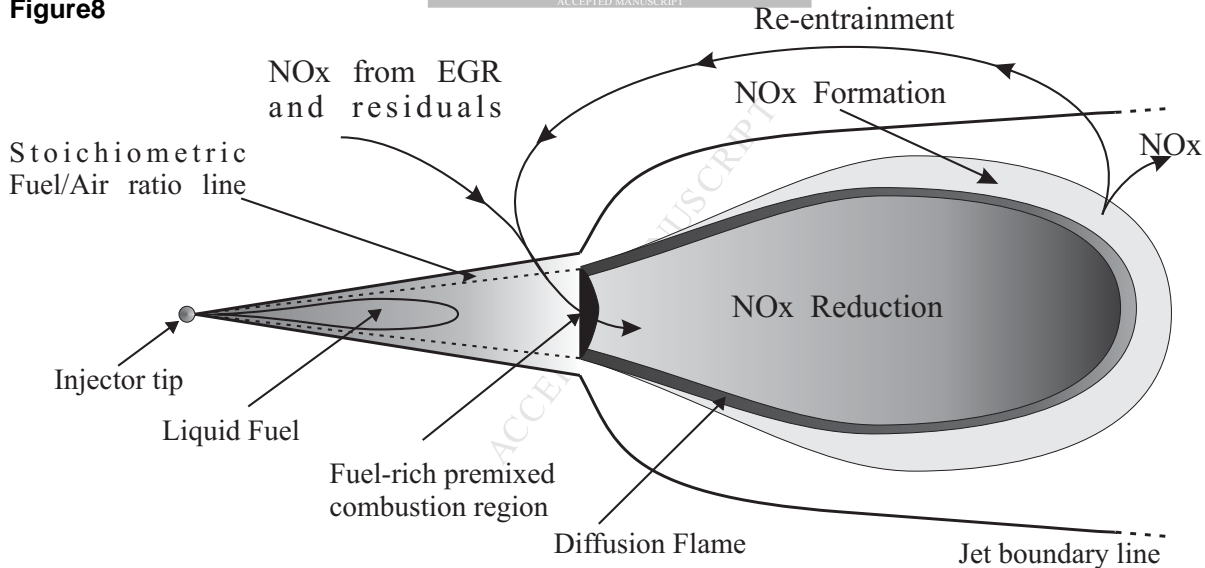
**Figure8**

Figure9

